

In situ angular measurements of thermal infrared sea surface emissivity—Validation of models

Raquel Niclòs*, Enric Valor, Vicente Caselles, César Coll, Juan Manuel Sánchez

Department of Thermodynamics, Faculty of Physics, University of Valencia, 50 Dr. Moliner, E-46100 Burjassot, Valencia, Spain

Received 22 April 2004; received in revised form 6 September 2004; accepted 8 September 2004

Abstract

In this paper, sea surface emissivity (SSE) measurements obtained from thermal infrared radiance data are presented. These measurements were carried out from a fixed oilrig under open sea conditions in the Mediterranean Sea during the WInd and Salinity Experiment 2000 (WISE 2000). The SSE retrieval methodology uses quasi-simultaneous measurements of the radiance coming from the sea surface and the downwelling sky radiance, in addition to the sea surface temperature (SST). The radiometric data were acquired by a CIMEL ELECTRONIQUE CE 312 radiometer, with four channels placed in the 8–14 μm region. The sea temperature was measured with high-precision thermal probes located on oceanographic buoys, which is not exactly equal to the required SST. A study of the skin effect during the radiometric measurements used in this work showed that a constant bulk–skin temperature difference of 0.05 ± 0.06 K was present for wind speeds larger than 5 m/s. Our study is limited to these conditions. Thus, SST used as a reference for SSE retrieval was obtained as the temperature measured by the contact thermometers placed on the buoys at 20-cm depth minus this bulk–skin temperature difference.

SSE was obtained under several observation angles and surface wind speed conditions, allowing us to study both the angular and the sea surface roughness dependence. Our results were compared with SSE models, showing the validity of the model of Masuda et al. [Masuda, K., Takashima, T., & Takayama, Y. (1988) Emissivity of pure seawaters for the model sea surface in the infrared window regions. *Remote Sensing of Environment*, 24, 313–329.] for observation angles up to 50° . For larger angles, the effect of double or multiple reflections on the sea surface produces discrepancies between measured and theoretical SSEs, and more complex models should be used to get accurate SSE values, such as the model of Wu and Smith [Wu, X., & Smith, W.L. (1997). Emissivity of rough sea surface for 8–13 μm : modelling and verification. *Applied Optics*, 36, 2609–2619.].

© 2004 Elsevier Inc. All rights reserved.

Keywords: Emissivity; Sea surface emissivity; Sea surface temperature; Thermal infrared; Angular measurements

1. Introduction

The requirement of a maximum uncertainty of ± 0.3 K in sea surface temperature (SST) as input to climate models and the use of high observation angles in the current space missions, such as the 55° for the forward view of the Advanced Along Track Scanning Radiometer (AATSR) (Llewellyn-Jones et al., 2001) on board ENVISAT, need a precise and reliable determination of sea

surface emissivity (SSE) in the thermal infrared region (TIR), as well as analyses of its angular and spectral dependences.

The emission of a rough sea surface has been studied over the last years due to the importance of the SSE for accurate SST retrieval. A reference work for many subsequent studies has been the paper written by Cox and Munk (1954), in which the sea surface roughness produced by the intensity of wind was characterized as an approximately normal and isotropic facet slope distribution. Saunders (1967) estimated the radiances emitted by a rough sea surface based on geometrical optics and the Cox and Munk (1954) distribution, observing that radiances from a

* Corresponding author. Tel.: +34 9635 43121; fax: +34 9635 43385.
E-mail address: Raquel.Niclos@uv.es (R. Niclòs).

rough sea surface are larger than those over a calm one. Later, Takashima and Takayama (1981) simulated emissivities of rough water surfaces as a function of wind speed up to 15 m/s for the Advanced Very High Resolution Radiometer (AVHRR) channels placed at 11 and 12 μm , and for observation angles of 0° and 55° . Sidran (1981) calculated rough sea surface emissivities and reflectivities for a large range of wavelengths, focusing the study on the angular reflection effect of the downwelling sky radiance. Then, Masuda et al. (1988) determined SSE for pure and seawaters in the spectral windows 3.5–4.1 and 8–13 μm as a function of the surface wind speed and the observation angle, results that have been extensively used for SST retrieval. With the use of the dual angle observation technique in current space missions, SSE at 55° for the forward view of the Along-Track Scanning Radiometer (ATSR) was studied by François and Otlé (1994), and simulated by Watts et al. (1996). However, the theoretical determination of SSE was later improved with the model developed by Wu and Smith (1997), where the effect of multiple surface reflections was taken into account.

In addition to theoretical models to understand the dynamics of SSE, ground measurements of SSE are needed. Liu et al. (1987) studied the surface emissivity variation with the suspended sediment concentrations, measuring surface emissivity of fresh (tap) and seawater samples at nadir with a 8–14 μm radiometer in the laboratory. They also observed that tap water emissivity is higher than seawater emissivity. Salisbury and D'Aria (1992) gave SSE experimental spectra within the region 8–14 μm for calm seawater measured also at nadir in the laboratory. Konda et al. (1994) determined sea surface emissivity using a 8–14 μm radiometer on an oceanographic tower placed in a bay of Japan. Measurements were carried out for a nadir view under high wind speed conditions. Smith et al. (1996) obtained SSE using radiance measurements collected with the Atmospheric Emitted Radiance Interferometer (AERI) Fourier transform

spectrometer placed on a ship under a wind speed of 5 m/s and three observation angles.

Nowadays the SSE determination is still a current issue mainly due to its importance for emissivity correction in algorithms to retrieve SST using off-nadir viewings of satellite sensors. Moderate and low resolution satellite sensors with channels in the TIR, such as the AVHRR on board NOAA and the Moderate Resolution Imaging Spectrometer (MODIS) (Barnes et al., 1998) on board EOS Aqua/Terra, have wide swaths in the across-track direction, and so the observation angles at the image edges are large, up to 55° for AVHRR and MODIS. Moreover, current satellite sensors permit observations centered on off-nadir angles in the along-track direction, such as the AATSR-ENVISAT at 55° or the future ESA mission Surface Processes and Ecosystem Changes Through Response Analysis (SPECTRA) with seven along-track directions between -60° and 60° . Table 1 shows a summary of experimental and theoretical SSE values at 55° for several wind speed conditions found in the bibliography. It shows the experimental values obtained by Smith et al. (1996) using the AERI, with an accuracy of $\pm 0.1\%$. Theoretical emissivities determined by Masuda et al. (1988), Watts et al. (1996) and Wu and Smith (1997) are also included in this table. Moreover, SSEs for an observation angle of 0° are given as reference in order to show the SSE decrease for an off-nadir observation, a fact that must be considered for accurate SST retrievals with the dual-angle technique. There are discrepancies between the SSE values given for 55° , mainly for high wind speed, which could cause SST uncertainties up to ± 0.5 K. Thus, additional SSE measurements are required in order to validate models and to select the most suitable model to retrieve accurate SSE values for any observation angle.

In this paper, we present SSE experimental values as a function of the observation angle and the surface wind speed for four channels placed in the TIR region: 8.2–9.2, 10.5–11.5, 11.5–12.5, and 8–14 μm . These SSE measurements were carried out from a fixed oilrig placed in the Mediterra-

Table 1

Experimental, E , and theoretical, T , SSE values for an observation angle of $\theta=55^\circ$ and several wind speeds, U , given by different sources

θ ($^\circ$)	Source	U (m/s)	8–14 μm	8.2–9.2 μm	10.5–11.5 μm	11.5–12.5 μm
55	Smith et al. (1996), E^a	5	0.962	0.961	0.9725	0.961
		15	0.962	0.959	0.971	0.959
	Masuda et al. (1988), T	5	0.966	0.963	0.974	0.962
		10	0.962	0.959	0.971	0.959
		15	0.960	0.957	0.968	0.956
	Watts et al. (1996), T^b	5	–	–	0.977	0.961
		10	–	–	0.976	0.960
		15	–	–	0.976	0.960
	Wu and Smith (1997), T	5	0.964	0.962	0.974	0.964
		10	0.964	0.962	0.973	0.964
15		0.965	0.963	0.974	0.965	
0	Salisbury and D'Aria (1992), E	–	0.985	0.984	0.990	0.986
	Masuda et al. (1988), T	–	0.987	0.985	0.991	0.988

These SSEs are integrated values for four classic TIR regions within the 8–14 μm (corresponding to the CE 312 radiometer, see Section 2).

^a Observation angle of 56.5° . Accuracy of $\pm 0.1\%$.

^b ATSR channels at 12 and 11 μm .

nean in the framework of the WInd and Salinity Experiment 2000 (WISE 2000) campaign (Camps et al., 2002), within the Soil Moisture and Ocean Salinity (SMOS) mission of ESA (Berger et al., 2002; Kerr et al., 2001).

In the next section, a description of the experimental site and the instrumentation is given. Section 3 presents in detail the proposed methodology for retrieving accurately sea surface emissivity, starting with a calibration procedure of the measurement system during the campaign and studying which measurements are required for SSE retrieval on the basis of the radiative transfer equation. Section 4 includes a sensitivity analysis of this methodology, and Section 5 shows the main results, analysing the performance of the SSE models and the implications of the SSE decrease for off-nadir observations. Finally, conclusions are summarized in Section 6.

2. Experimental site and instrumentation

The WInd and Salinity Experiment 2000 (WISE 2000) was carried out in the framework of the Soil Moisture and Ocean Salinity (SMOS) mission, sponsored by the European Space Agency (ESA). This campaign was held from 15 November 2000 to 13 January 2001 at the Repsol-YPF's Casablanca fixed oilrig, avoiding the swinging problems of instrumentation mounted on research vessels. It is placed at $40^{\circ}43' 4''\text{N}$ and $1^{\circ}21' 34''\text{E}$, 40 km off the mouth of the River Ebro on the coast of Tarragona, Spain (Fig. 1). In this location, the sea conditions are representative of the open Mediterranean with periodic influence of the River Ebro freshwater plume.

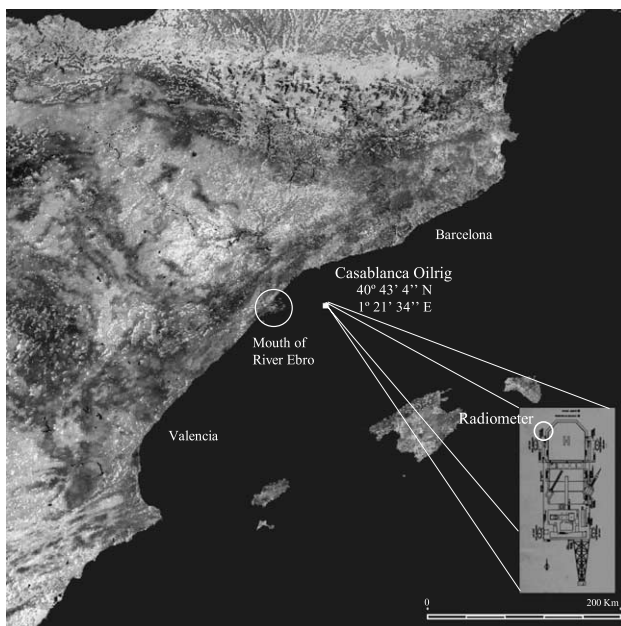


Fig. 1. Casablanca oilrig situation in the Western Mediterranean, near the eastern coast of the Iberian Peninsula. A detail of the radiometer position and orientation during the WISE campaign is also included.

The TIR measurements of sea surface and sky were made with the radiometer CIMEL ELECTRONIQUE model CE 312 (Legrand et al., 2000; Sicard et al., 1999). It has four spectral channels: one broad, 8–14 μm (band 1), and three narrow channels, 8.2–9.2, 10.5–11.5, and 11.5–12.5 μm (bands 4, 3 and 2, respectively). The radiometer has a field of view of 10° , a response time of 1 s, and precisions of ± 0.10 , ± 0.12 , ± 0.09 and ± 0.14 K for channels 1–4, respectively (Niclòs et al., 2004). The cavity containing the detector is used as a temperature reference. A platinum probe attached to the detector surface monitors the internal temperature of the head. The radiometer is provided with a concealable, gold-coated mirror, which allows comparisons between the radiance coming from an external target and from the optical head cavity in order to check and correct any possible variations in the temperature of the optical head that could affect the measurements.

During the campaign, the CE 312 radiometer was measuring continuously, recording one measurement every 2.5 min. Its optical head was fixed on a mobile pedestal and placed on an external terrace in the north oilrig side at 32-m height over the sea (Figs. 1 and 2a, b). The pedestal motor allowed us to point the sensor with a high-accuracy inclinometer. In this way, scan processes of about 30 min were carried out, measuring the TIR radiance of the sea surface for observation angles of 25° , 35° , 45° , 55° and 65° , alternately with the sky radiance. Areas of the footprints on the sea surface due to the radiometer field of view for each observation angle, and ranges of emission angles within these footprints, are provided in Table 2. These area centers are shifted from the point corresponding to the observation angle when this angle increases, and so the areal average emission angle is slightly larger than the pointing angle (i.e. the average emission angle is 65.8° for an observation angle of 65°).

The CE 312 radiometer was kept in a shelter to be protected from the environmental conditions of open sea (Fig. 2c) and the incoming radiance was observed through a ZnSe window 4 mm thick, which was selected because of its good transmission in the TIR region. A small bag of silica gel was placed inside the protective shelter to prevent the formation of condensation drops. To take into account the effect of the optical properties of this window, calibrations of the complete system (protective shelter and radiometer) were carried out (see Section 3.1).

Simultaneous measurements of the sea temperature and surface wind speed were carried out during the campaign. Sea temperature was given by Sea-Bird Electronics (SBE) 37-SM MicroCAT thermal probes placed in oceanographic buoys measuring at 20-cm depth. These thermal probes are high-precision thermistors, providing an accuracy of ± 0.002 K after manufacturer calibrations previous to the campaign (Budeus & Schneider, 1998; Font et al., 2003). The buoys were located very close to the thermal radiometer target and collected measurements

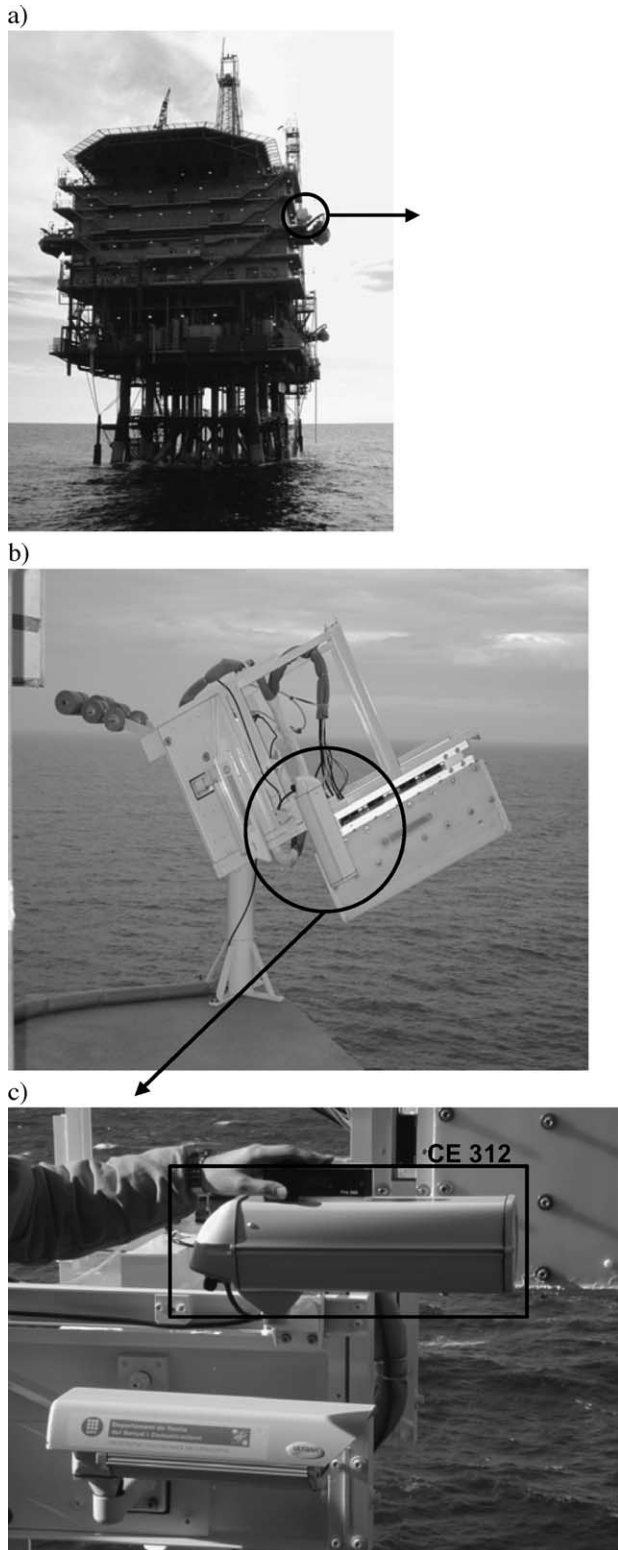


Fig. 2. (a) General view of the Casablanca oilrig; (b) the radiometer mobile pedestal on an external terrace; and (c) a detail of the protective shelter containing the CE 312 optical head.

every 2 min. Surface wind speed was measured using calibrated anemometers placed on these oceanographic buoys with an error of ± 0.9 m/s, providing wind speed

data at 12.5-m height, which is considered as the reference height for surface wind speed in the theoretical models (Cox & Munk, 1954; Masuda et al., 1988; Wu & Smith, 1997).

3. Methodology

3.1. Calibration

A black-body calibration source was used as a reference for the calibration procedure of the radiometer closed in the protective shelter and viewing through the ZnSe window. Extensive calibration processes were carried out before and after the campaign, and also additional calibration measurements were performed one time per scan process. The calibration source temperature was collected using an internal temperature probe.

A calibration function was obtained for each channel (Nicolòs et al., 2004) and the calibrated brightness temperature, T_s , was obtained as:

$$B_i(T_s) = \frac{R_{m,i} + (\tau_{w,i} - 1)B_i(T_{in}) - \zeta_i}{\tau_{w,i}} \quad (1)$$

where $R_{m,i}$ is the CE 312 radiance measured through the ZnSe window of the protective shelter in channel i ; $B_i(T)$ is the channel i averaged Planck's function for a temperature T ; T_{in} is the internal temperature of the radiometer's optical head; $\tau_{w,i}$ is the window transmittance; and ζ_i is a constant for each channel. Full details on the calibration procedure are given in Nicolòs et al. (2004). The calibration coefficients, $\tau_{w,i}$ and ζ_i , obtained for WISE 2000 are presented in Table 3.

After performing the calibration of the CE 312 data measured during the campaign, sea surface radiance errors of $\pm 2.0 \times 10^{-5}$, $\pm 2.7 \times 10^{-5}$, $\pm 1.9 \times 10^{-5}$ and $\pm 2.2 \times 10^{-5}$ mW/(cm² sr cm⁻¹) were obtained for the CE 312 channels 1 to 4, respectively (i.e. ± 0.14 , ± 0.16 , ± 0.12 and ± 0.18 K, respectively, in terms of temperature).

3.2. Sea surface emissivity determination

The radiance measured by channel i of a TIR radiometer located at a height h and observing the sea surface under a

Table 2

Areas of the observed footprint at the sea surface for each observation angle, θ , and ranges of emission angles within each footprint, $\Delta\theta_e$, due to the radiometer field of view of 10°

θ ($^\circ$)	Observed area (m ²)	$\Delta\theta_e$ ($^\circ$)	θ_e ($^\circ$)
25	31.8	20–30	25.2
35	42.4	30–40	35.3
45	64.5	40–50	45.4
55	117.8	50–60	55.5
65	284.7	60–70	65.8

The average emission angles, θ_e , for these areas observed by the radiometer are also provided.

Table 3

Calibration coefficients, $\tau_{w,i}$ and ζ_i (Eq. (1)), and their standard deviations, $\sigma(\tau_{w,i})$ and $\sigma(\zeta_i)$, respectively, obtained for the CE 312 channels

CE 312 channel	$\tau_{w,i}$	$\pm\sigma(\tau_{w,i})$	ζ_i (mW/(cm ² sr cm ⁻¹))	$\pm\sigma(\zeta_i)$ (mW/(cm ² sr cm ⁻¹))	r^2
1 (8–14 μm)	0.726	0.006	-12.0×10^{-6}	0.9×10^{-6}	0.991
4 (8.2–9.2 μm)	0.768	0.018	-18×10^{-6}	2×10^{-6}	0.939
3 (10.5–11.5 μm)	0.745	0.008	-15.6×10^{-6}	1.3×10^{-6}	0.986
2 (11.5–12.5 μm)	0.735	0.014	-23×10^{-6}	2×10^{-6}	0.955

r^2 is the determination coefficient for each linear regression.

direction (θ, ϕ) , $R_i(\theta, \phi, h)$, is the sum of three contributions: (i) direct emission of the sea surface, which is attenuated by the absorption of the atmospheric layer between the sea surface and the instrument; (ii) reflection of the downwelling sky radiance on the sea, attenuated by the atmosphere; and (iii) the upwelling atmospheric radiance emitted in the observing direction. Thus, the measured radiance can be expressed as:

$$R_i(\theta, \phi, h) = \varepsilon_i(\theta, \phi)B_i(\text{SST})\tau_i(\theta, \phi, 0, h) + [1 - \varepsilon_i(\theta, \phi)]L_i^{\downarrow \text{atm}}(\bar{\theta}_r, \phi)\tau_i(\theta, \phi, 0, h) + L_i^{\uparrow \text{atm}}(\theta, \phi, 0, h) \quad (2)$$

where $B_i(\text{SST})$ is the channel i averaged Planck's function for a skin temperature SST; $\varepsilon_i(\theta, \phi)$ is the sea surface emissivity; $\tau_i(\theta, \phi, 0, h)$ and $L_i^{\uparrow \text{atm}}(\theta, \phi, 0, h)$ are the transmittance and the radiance emitted upwards by the atmospheric layer between sea surface and sensor; and $\bar{\theta}_r$ is an effective angle such that $L_i^{\downarrow \text{atm}}(\bar{\theta}_r, \phi)$ equals the angular integration of the downwelling sky radiance for all the different directions that contribute to the signal sensed at θ direction due to the sea roughness effect. Sidran (1981) evaluated the error introduced by the approximation of using the complementary angle to θ in the calculation of the reflection for a rough sea surface, showing that the effect on the retrieved SST was negligible ($< \pm 0.05$ K). Thus, the approximation $\bar{\theta}_r = \pi - \theta$ has been considered in this work.

Eq. (2) allows the recovery of $\varepsilon_i(\theta, \phi)$ from the radiometer measurements, $R_i(\theta, \phi, h)$, and the atmospheric parameters, if SST is known. Therefore, SSE can be obtained from Eq. (2) as:

$$\varepsilon_i(\theta, \phi) = \left[R_i(\theta, \phi, h) - \tau_i(\theta, \phi, 0, h) L_i^{\downarrow \text{atm}}(\pi - \theta, \phi) - L_i^{\uparrow \text{atm}}(\theta, \phi, 0, h) \right] / \left\{ \tau_i(\theta, \phi, 0, h) \left[B_i(\text{SST}) - L_i^{\downarrow \text{atm}}(\pi - \theta, \phi) \right] \right\} \quad (3)$$

Taking into account the optical path between the sea surface and the radiometer (from 35 m at $\theta=25^\circ$ to 76 m at $\theta=65^\circ$), this atmospheric layer can be considered approximately transparent and with a negligible emission for CE 312 channels, mainly for channels 2 and 3 (see Fig. 3a and b). $\tau_i(\theta, \phi, 0, h)$ and $L_i^{\uparrow \text{atm}}(\theta, \phi, 0, h)$ were evaluated using local air pressure, temperature and relative humidity data measured at different altitudes at the oilrig

during the campaign. These data were introduced into the MODTRAN 4 code (Berk et al., 1999) to get estimates of both $\tau_i(\theta, \phi, 0, h)$ and $L_i^{\uparrow \text{atm}}(\theta, \phi, 0, h)$ (Niclòs et al., 2004). Average transmittance values of 0.979 ± 0.005 , 0.983 ± 0.005 , 0.993 ± 0.002 , and 0.977 ± 0.006 were

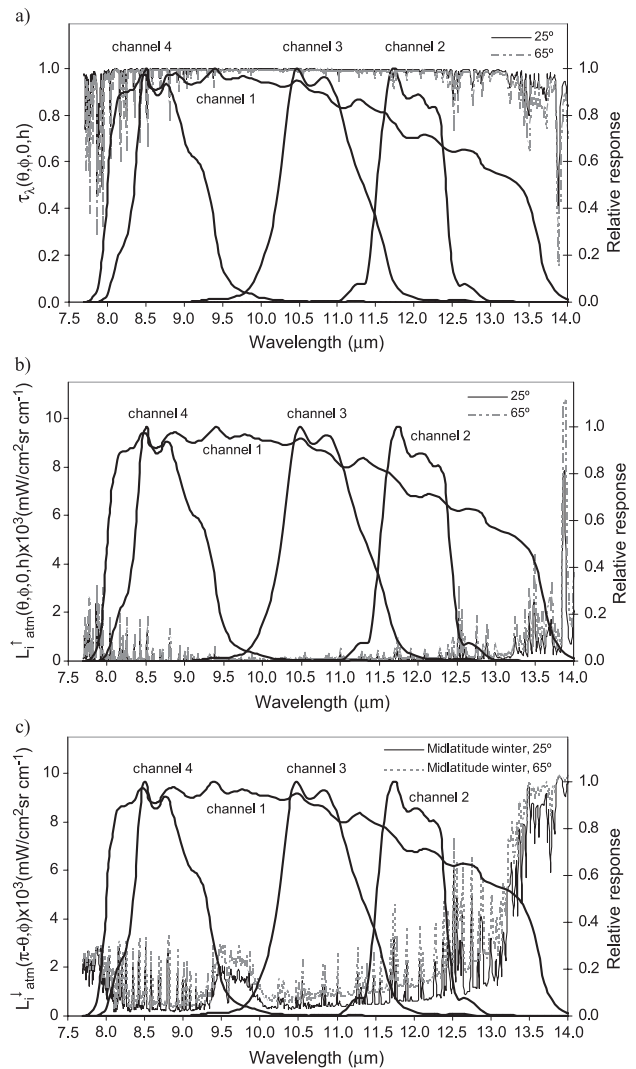


Fig. 3. (a) Transmittance for the atmospheric layer between the sea surface and the radiometer. (b) Upwelling sky radiance emitted by the layer between the sea surface and the radiometer, obtained with the MODTRAN 4 code and using local pressure, relative humidity and temperature. (c) Downwelling sky radiance emitted by the whole atmosphere simulated for a midlatitude summer standard atmosphere. The spectral response functions of the CE 312 radiometer channels are shown in the secondary axis of all these plots.

obtained for CE 312 channels 1 to 4, respectively. Also average values for the upwelling atmospheric radiance of $(1.5 \pm 0.4) \times 10^{-4}$, $(1.8 \pm 0.6) \times 10^{-4}$, $(0.7 \pm 0.2) \times 10^{-4}$, and $(1.2 \pm 0.3) \times 10^{-4}$ mW/(cm² sr cm⁻¹) were obtained for channels 1 to 4, respectively (see Fig. 3a and b). These data represent average values and their deviation for the considered observation angles, i.e. from 25° to 65°.

However, the downwelling sky radiance, coming from the atmosphere as a whole, cannot be neglected, since its value is more similar to the sea surface radiance, but it should be directly measured (Nicolòs et al., 2004). Fig. 3c shows the spectral downwelling sky radiance for a midlatitude summer standard atmosphere, which is a little lower than the values measured during the campaign.

The use of the approximation $\tau_i(\theta, \phi, 0, h) \approx 1$ and $L_i^{\uparrow \text{atm}}(\theta, \phi, 0, h) \approx 0$ in Eq. (3) cause systematic errors in terms of emissivity, with average values of 0.00232 ± 0.00016 , 0.0001 ± 0.0004 , 0.00042 ± 0.00005 , and 0.0034 ± 0.0004 for channels 1 to 4, respectively, where the reported deviations indicate again the variability with the observation angles. These results show that the atmospheric correction effect is practically negligible for the emissivity determination especially for channels 2 and 3.

$R_i(\theta, \phi, h)$ and $L_i^{\downarrow \text{atm}}(\pi - \theta, \phi)$ measurements were carried out alternatively by the CE 312 radiometer using observation angles of θ and $\pi - \theta$, respectively. $\tau_i(\theta, \phi, 0, h)$ and $L_i^{\uparrow \text{atm}}(\theta, \phi, 0, h)$ were simulated for each angle using local profiles in the MODTRAN code. Sea temperature was measured simultaneously by the thermal probes placed on the oceanographic buoys. There is ample evidence of the existence of a difference between the temperatures measured by contact thermometers (placed at 20-cm depth in this case) and the temperatures measured with thermal infrared radiometers, which correspond to the first few micrometers of the sea surface (Donlon et al., 1999; Harris et al., 1994; Konda et al., 1994; Murray et al., 2000; Robinson et al., 1984; Saunders, 1967). The so-called bulk–skin temperature difference depends on the wind speed and the net heat flux at the sea surface (Wick et al., 1996), and may take values from +1.0 to -1.0 K (Schluessel et al., 1990). At night, the skin effect is usually positive, i.e. there is a cold skin as a result of an evaporative cooling. At daytime, it may have both signs for low wind speeds (Donlon et al., 2002). However, bulk–skin temperature difference seems to tend to a constant value of about 0.2 K for wind speeds larger than 5–7 m/s (Donlon et al., 2002; Konda et al., 1994; Murray et al., 2000; Wick et al., 1996). This skin effect was studied during the campaign for wind speed values larger than 5 m/s. The bulk temperature was measured by the contact thermometers at 20-cm depth and the skin temperature was determined using radiometric data measured by the CE 312 channel 3 (10.5–11.5 μm) at 25°. This configuration was selected in Nicolòs et al. (2004) as the most accurate procedure in order to measure SST, since atmospheric and emissivity effects were minima for this spectral and angular conditions and also errors

introduced by the input magnitudes caused the minimum SST error. The comparison of these data during the selected measurements for SSE retrieval showed an experimental bulk–skin temperature difference of 0.05 ± 0.06 K for wind speed larger than 5 m/s, which is lower than the skin effect values found in the bibliography measured at different depth and sea conditions. Taking into account these results, we limited our study to situations with wind speed values larger than 5 m/s, for which the sea temperature measured by the thermal probes placed in buoys can be used as reference temperature for SSE retrieval if this constant bulk–skin temperature difference is subtracted. The buoy probes measured the sea temperature every 2 min, but SST values measured by the radiometer under these optimum conditions (25° and channel 3) were obtained once per scan process (i.e. in 30-min periods). Thus, the reference SST was determined from the buoy measurements, to which the constant skin effect was subtracted, since their large frequency permitted us to control possible SST fluctuations during each scan process.

Other limitations that were considered in the scan processes selection to obtain the most accurate SSE values were related with:

- (i) Variability of the sky conditions: this becomes an important factor when the sky temperature is close to the SST, e.g. in the case of low and warm clouds, when an error of a few tenths in the sky temperature causes an SSE error of about $\pm 1\%$. In order to minimize this error source, the SSE measurements were made only under cloud-free sky conditions, or in the case of high and cold clouds due to their small influence.
- (ii) Foam effect: we limited our study for wind speeds ≤ 10 m/s in order to avoid possible effects due to foam coverage. The foam coverage was determined during the WISE 2000 campaign using video frames from a camera mounted close to the radiometer that observed the measurement area for each angle (Camps et al., 2002; Villarino et al., in press). For wind speeds up to 10 m/s, the determined sea foam percent coverage was lower than 1% in all cases. For 15 m/s, this foam coverage increased to 3%. Thus, we limited our study to wind speed values up to about 10 m/s, for which foam coverage was negligible. On the other hand, conditions of wind speeds larger than 10 m/s rarely coincided with clear skies and therefore insufficient matchups were available to determine SSE angular variation under these wind speed values.
- (iii) Wind direction: as the radiometer was pointing approximately to the north from the north side of the platform, only scan processes carried out under west winds, perpendicular to the pointing direction, were used in order to avoid effects of wind shadowing due to the oilrig. The predominant wind direction in the oilrig location during the campaign was NW.

4. Sensitivity analysis

The main error sources in the SSE determination by means of this methodology are the following:

- (i) CE 312 radiometric error and system calibration error, described in Sections 2 and 3.1.
- (ii) SST measurement error, $\sigma(\text{SST})$: SST was obtained by subtracting the skin effect of 0.05 ± 0.06 K to the buoy thermal probes measurements. Thus, $\sigma(\text{SST})$ was determined from the standard deviation obtained in the skin effect, ± 0.06 K.
- (iii) System pointing error: the radiometer pointing inclinometer error was $\pm 0.01^\circ$; however, an error of $\pm 0.5^\circ$ is considered for this study, which would include any possible sensor movement due to the wind effect and vibrations of the fixed oilrig.
- (iv) Error in the atmospheric correction terms: since $\tau_i(\theta, \phi, 0, h)$ and $L_i^{\uparrow \text{atm}}(\theta, \phi, 0, h)$ were estimated introducing local pressure, temperature and humidity data into the MODTRAN 4 code, errors of estimate of these atmospheric terms were obtained as a consequence of the experimental errors of these meteorological data.
- (v) Possible existence of SST horizontal thermal gradients: the SST variability was checked before each process by changing slightly the azimuth observation angle showing negligible horizontal thermal gradients through and around the target.

Thus, SSE precision, $\sigma(\varepsilon_i(\theta, \phi))$, is derived taking into account error sources (i)–(iv). Applying error theory to Eq. (3), $\sigma(\varepsilon_i(\theta, \phi))$ is written as:

$$\begin{aligned} \sigma(\varepsilon_i(\theta, \phi)) = & \left\{ \left[\frac{\partial \varepsilon_i(\theta, \phi)}{\partial R_i(\theta, \phi, h)} \sigma(R_i(\theta, \phi, h)) \right]^2 \right. \\ & + \left[\frac{\partial \varepsilon_i(\theta, \phi)}{\partial L_i^{\downarrow \text{atm}}(\pi - \theta, \phi)} \sigma(L_i^{\downarrow \text{atm}}(\pi - \theta, \phi)) \right]^2 \\ & + \left[\frac{\partial \varepsilon_i(\theta, \phi)}{\partial B_i(\text{SST})} \sigma(B_i(\text{SST})) \right]^2 \\ & + \left[\frac{\partial \varepsilon_i(\theta, \phi)}{\partial \tau_i(\theta, \phi, 0, h)} \sigma(\tau_i(\theta, \phi, 0, h)) \right]^2 \\ & + \left. \left[\frac{\partial \varepsilon_i(\theta, \phi)}{\partial L_i^{\uparrow \text{atm}}(\theta, \phi, 0, h)} \right. \right. \\ & \left. \left. \times \sigma(L_i^{\uparrow \text{atm}}(\theta, \phi, 0, h)) \right]^2 \right\}^{\frac{1}{2}} \end{aligned} \quad (4)$$

where $\sigma(B_i(\text{SST}))$ is the error of Planck's function for the SST, which can be obtained from $\sigma(\text{SST})$ as:

$$\sigma(B_i(\text{SST})) = \left| \frac{\partial B_i(\text{SST})}{\partial \text{SST}} \right| \sigma(\text{SST}) \quad (5)$$

obtaining average values of $\pm 8 \times 10^{-6}$, $\pm 1.0 \times 10^{-5}$, $\pm 9 \times 10^{-6}$ and $\pm 7 \times 10^{-6}$ mW/(cm² sr cm⁻¹) for channels 1 to 4, respectively.

$\sigma(\tau_i(\theta, \phi, 0, h))$ and $\sigma(L_i^{\uparrow \text{atm}}(\theta, \phi, 0, h))$ were estimated using the MODTRAN code by modifying local pressure, humidity and temperature data according to their experimental errors, i.e. ± 1 mb, $\pm 2\%$ and ± 0.1 K, respectively. Transmittance errors of $\pm 0.10\%$, $\pm 0.14\%$, $\pm 0.06\%$, $\pm 0.10\%$ were estimated for channels 1 to 4, and errors of $\pm 3.9\%$, $\pm 5.6\%$, $\pm 6.5\%$, and $\pm 3.5\%$ were obtained for $\sigma(L_i^{\uparrow \text{atm}}(\theta, \phi, 0, h))$.

$\sigma(R_i(\theta, \phi, h))$ and $\sigma(L_i^{\downarrow \text{atm}}(\pi - \theta, \phi))$ are obtained independently from both radiometric-calibration error, σ_{rci} , and the system pointing error, σ_θ , as:

$$\sigma_i^2 = \sigma_{\text{rci}}^2 + \sigma_{\theta i}^2 \quad (6)$$

CE 312 radiometric error and system calibration error are considered from Eq. (1) (Niclòs et al., 2004), which yields σ_{rci} for both $R_i(\theta, \phi, h)$ and $L_i^{\downarrow \text{atm}}(\pi - \theta, \phi)$. The system pointing error, $\sigma_{\theta i}$, is obtained from the dependence of $R_i(\theta, \phi, h)$ and $L_i^{\downarrow \text{atm}}(\pi - \theta, \phi)$ with the observation angle. Polynomial regressions between $R_i(\theta, \phi, h)$ and θ , and $L_i^{\downarrow \text{atm}}(\pi - \theta, \phi)$ and θ , were determined for each measurement process and channel, obtaining determination coefficients, r_i^2 , higher than 0.95 in all cases. From these regression equations, the pointing errors can be calculated as:

$$\sigma_{\theta i} = \left| \frac{\partial R_i}{\partial \theta} \right| \sigma(\theta) \quad (7)$$

Average SSE errors of ± 0.004 , ± 0.004 , ± 0.003 and ± 0.006 were finally obtained for CE 312 channels 1 to 4, respectively. The spectral variation of these SSE errors is due mainly to the implicit radiometric error for each band of the CE 312 radiometer.

5. Results and analysis

Sea surface emissivity was determined for observation angles from 25° to 65° , at steps of 10° , by means of the described methodology. Measurements of simultaneous sea surface radiance, sky radiance and sea surface temperature were used for this aim.

Table 4 shows the retrieved SSEs as a function of the observation angle, θ , for two values of the surface wind speed ($U=5$ and 10 m/s approximately) and for each CE 312 channel. These SSEs are average values of all the measurement processes carried out during the campaign. The highest SSE values and the lowest SSE errors, $\sigma(\text{SSE})$, are obtained for CE 312 channel 3 (10.5–11.5 μm).

Fig. 4 shows the angular dependence of the average SSE values experimentally obtained during WISE 2000 under surface wind speeds, U , close to 5 m/s (with a mean value of

Table 4

Sea surface emissivity (SSE) values obtained for each CE 312 channel at different observation angles, θ , and surface wind speeds, U

U (m/s)	θ (°)	Ch1 (8–14 μm)		Ch4 (8.2–9.2 μm)		Ch3 (10.5–11.5 μm)		Ch2 (11.5–12.5 μm)	
		SSE	σ (SSE)	SSE	σ (SSE)	SSE	σ (SSE)	SSE	σ (SSE)
5	25	0.986	0.004	0.987	0.004	0.991	0.003	0.985	0.005
	35	0.984	0.004	0.985	0.004	0.989	0.003	0.983	0.005
	45	0.978	0.004	0.978	0.004	0.985	0.003	0.976	0.006
	55	0.964	0.004	0.961	0.005	0.973	0.003	0.961	0.006
	65	0.932	0.005	0.927	0.006	0.944	0.003	0.927	0.007
10	25	0.986	0.004	0.987	0.004	0.991	0.003	0.985	0.005
	35	0.984	0.004	0.984	0.004	0.990	0.003	0.983	0.005
	45	0.977	0.004	0.977	0.004	0.984	0.003	0.978	0.005
	55	0.963	0.004	0.961	0.004	0.973	0.003	0.962	0.006
	65	0.933	0.004	0.926	0.005	0.946	0.003	0.929	0.006

σ (SSE) is the SSE error, i.e. the maximum value between the error calculated by means of Eqs. (4)–(7) and the standard deviation obtained from the several measurement processes carried out during the campaign.

4.5 ± 0.9 m/s) and 10 m/s (10.3 ± 1.1 m/s) for the CE 312 channels. For comparison, Fig. 4 presents also the corresponding theoretical SSE values calculated by means of the

model of Masuda et al. (1988) for surface wind speed values of 5 and 10 m/s. This figure shows that SSE decreases with the observation angle, with a reduction of 2–3% for 55°.

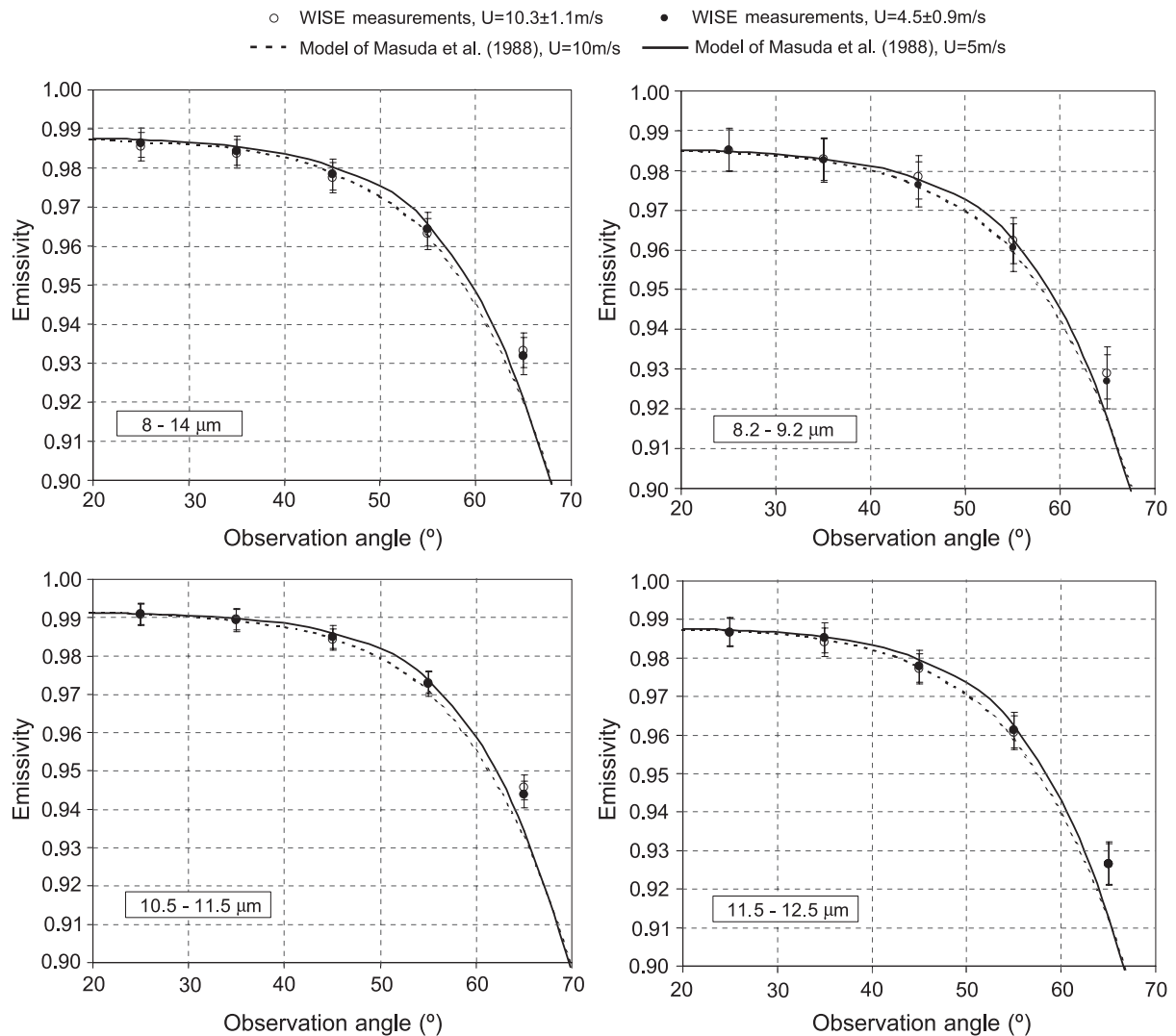


Fig. 4. Angular variation of the sea surface emissivity. Comparison between the experimental values and the theoretical SSEs of the model of Masuda et al. (1988).

This fact is important for biangular measurements with instruments such as AATSR, since such an error on SSE will cause an error of about 1.2 K on SST (François & Ottlé, 1994).

Fig. 4 also proves the validity of the model of Masuda et al. (1988) for observation angles up to about 50°, where the differences between measured and theoretical SSEs are within the experimental errors. However, there are discrepancies for observation angles larger than 50°. SSE computed by the model is smaller than the in situ measured values for $\theta=65^\circ$, and these differences seem to increase slightly with the surface wind speed. The model of Masuda et al. (1988) neglects the effect of multiple reflections, i.e. the reflection probability of the radiance emitted by the sea surface on itself for high observation angles and wind speeds. Double reflections of the downwelling sky radiance could also be possible, contributing to the signal sensed by the radiometer. These

effects could explain the discrepancies with regard to the model of Masuda et al. (1988) under large observation angles and wind speeds, which were already pointed out by Watts et al. (1996) and Wu and Smith (1997). The model of Masuda et al. (1988) predicts a reduction of SSE with wind speed (i.e. with sea surface roughness) for observation angles up to 70°. This reduction is not shown in our measurements, which even suggest an SSE increase with wind speed for angles larger than 60°. Fig. 5 compares the experimental values with the Wu and Smith emissivities, and also shows values measured by Smith et al. (1996) using the Atmospheric Emitted Radiance Interferometer (AERI) Fourier transform spectrometer placed on a ship, for which they gave an accuracy of $\pm 0.1\%$. Mean wind speed at the time of observation was 5 m/s, and measurements were performed at 36.5°, 56.5° and 73.5° from nadir (Smith et al., 1996). A better agreement between theory and measurements for high observation

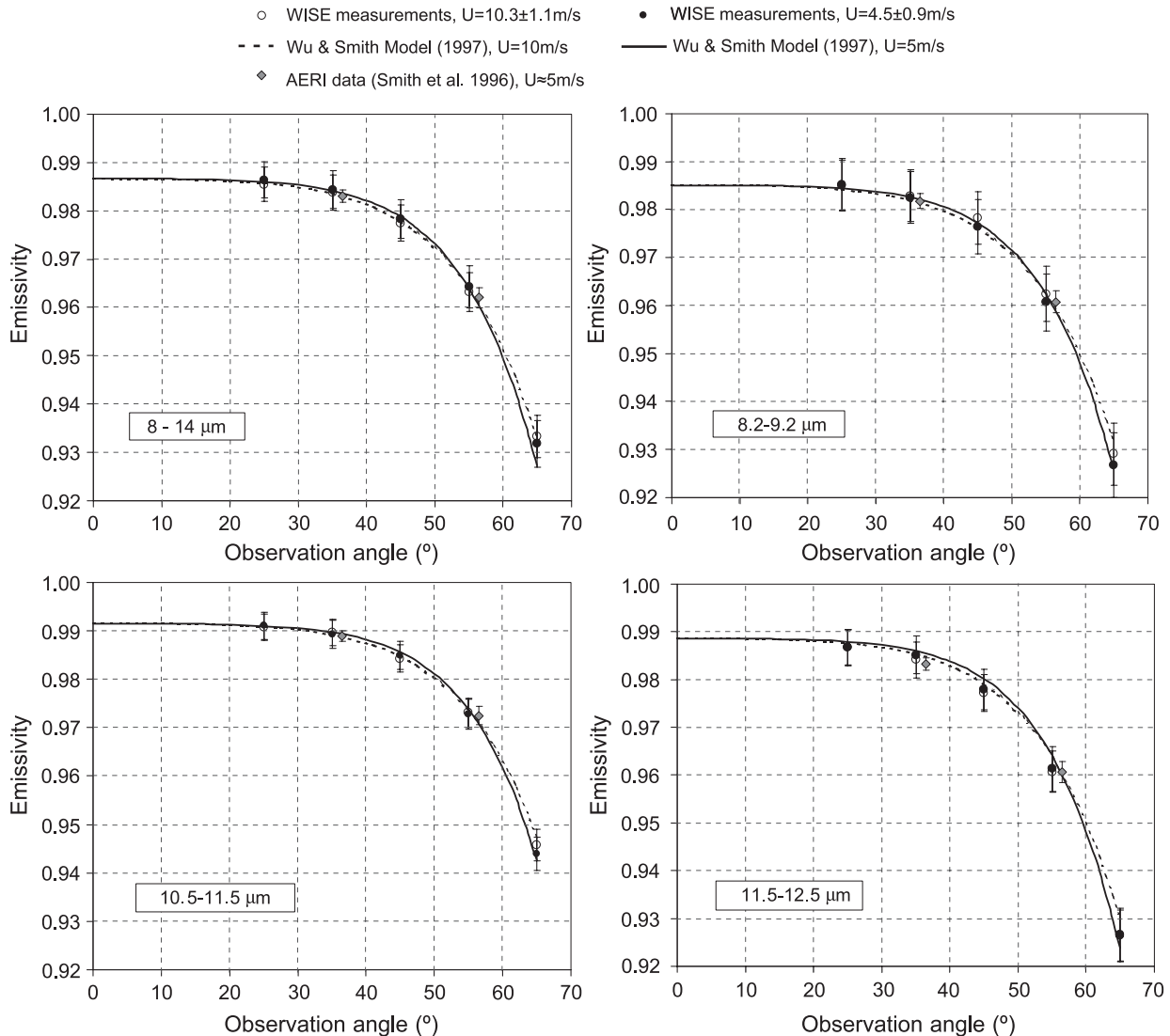


Fig. 5. Comparison between the experimental values, and the theoretical SSEs of the model of Wu and Smith (1997). Measurements with AERI (Smith et al., 1996) for wind speed conditions of about 5 m/s are also shown.

angles is shown, where the reverse SSE dependence with wind speed is observed for both experimental and theoretical values. This fact is due to the multiple reflection effects, which produce a reduction of the SSE sensitivity to the sea surface roughness at small to moderate observation angles and an amplification of the SSE increase with wind speed for angles higher than 60° (Wu and Smith, 1997).

In this case, the measured–theoretical SSE differences are within the experimental errors for all the observation angles, which proves the soundness of the model of Wu and Smith (1997) even for large observation angles.

6. Conclusions

Angular measurements of SSE in the TIR region under open sea conditions are presented in this work. The methodology consists of quasi-simultaneous measurements of the radiance coming from the sea surface and the downwelling sky radiance, both measured by a CE 312 radiometer with four channels in the TIR. In addition, the reference SST is determined using values measured by high-precision thermal probes located on oceanographic buoys corrected for the skin effect, which was determined to be 0.05 ± 0.06 K for the high wind speed conditions.

SSEs were obtained under observation angles from 25° to 65° , at steps of 10° , and two surface wind speed conditions (5 and 10 m/s approximately). Using the described methodology, SSEs were attained with average errors of ± 0.004 , ± 0.004 , ± 0.003 and ± 0.006 for CE 312 channels 1–4, respectively.

The good agreement found between these experimental values and the model of Masuda et al. (1988) at small to moderate observation angles confirms the validity of this model to determine SSE for a nadir sea surface observation. However, discrepancies appear for large observation angles due to the omission of the effect of double and multiple reflections on the sea surface by the model of Masuda et al. (1988). This effect produces a reduction of the SSE sensitivity to the sea surface roughness at small to moderate observation angles and an amplification of the SSE increase with wind speed for angles higher than 60° . This fact was taken into account by models such as the one proposed by Wu and Smith (1997), which shows SSE values in agreement with the experimental measurements, proving its soundness for all the measured observation angles, and so its reliability to obtain SSE for off-nadir viewings.

Acknowledgements

This work was supported by the European Space Agency through the WISE 2000 and WISE 2001 campaigns (ESTEC Contract 14188/00/NL/DC), the Spanish Ministerio de Educación y Ciencia (Project REN2001-3116/CLI, and

“Ramón y Cajal” Research Contract of Dr. E. Valor), the European Union (FEDER funds), and the Generalitat Valenciana (Project GV2004-B-084). The Spanish Ministerio de Educación, Cultura y Deporte is also acknowledged for the Research Grant received by R. Niçlòs.

We thank Dr. J. Font (ICM-CSIC, Barcelona, Spain), Prof. A. Camps (TSC-UPC, Barcelona, Spain), Dr. J. Etcheto (LODYC-IPSL, Paris, France) and R. Rivas (IHLLA, Buenos Aires) for their assistance during WISE campaigns. The collaboration of Dr. E. Rubio (UCLM, Albacete, Spain) and L. Martínez (ICC, Barcelona, Spain), who took part in the preparation of the campaign, is also appreciated. Finally, we would like to thank the assistance of P. van Delst (NOAA/NCEP/EMC, Camp Springs MD, USA) regarding to the computed spectral emissivities of the model of Wu and Smith.

Finally, the suggestions and comments made by anonymous reviewers are also acknowledged.

References

- Barnes, W. L., Pagano, T. S., & Salomonson, V. V. (1998). Prelaunch characteristics of the Moderate Resolution Imaging Spectroradiometer (MODIS) on EOS-AM1. *IEEE Transactions on Geoscience and Remote Sensing*, 36(4), 1088–1100.
- Berger, M., Camps, A., Font, J., Kerr, Y., Miller, J., Johannessen, J., et al. (2002). Measuring ocean salinity with ESA's SMOS mission. *ESA Bulletin*, 111, 113–121.
- Berk, A., Anderson, G. P., Acharya, P. K., Chetwynd, J. H., Bernstein, L. S., Shettle, E. P., et al. (1999). MODTRAN 4 user's manual. Air Force Research Laboratory, Space Vehicles Directorate, Air Force Materiel Command, Hascom AFB, MA, 95 pp.
- Budeus, G., & Schneider, W. (1998). In-situ temperature calibration: A remark on instruments and methods. *International WOCE Newsletter*, 30, 16–18.
- Camps, A., Font, J., Etcheto, J., Rubio, E., Weill, A., Corbella, I., et al. (2002). Sea surface emissivity observations at L-band: First results of the wind and salinity experiment WISE-2000. *IEEE Transactions on Geoscience and Remote Sensing*, 40(10), 2117–2130.
- Cox, C., & Munk, W. (1954). Some problems in optical oceanography. *Journal of Marine Research*, 14, 63–78.
- Donlon, C. J., Minnet, P. J., Gentemann, C., Nightingale, T. J., Barton, I. J., Ward, B., et al. (2002). Toward improved validation of satellite sea surface skin temperature measurements for climate research. *Journal of Climate*, 15, 353–369.
- Donlon, C. J., Sheasby, T., Turner, J., Robinson, I. S., & Emery, W. J. (1999). Implications of the oceanic thermal skin temperature derivation at high wind speed. *Geophysical Research Letters*, 26, 2505–2508.
- Font, J., Gabarró, C., Julià, A., Emelianov, M., Lloret, M. I., Etcheto, J., et al. (2003). Oceanographic conditions during the Wind and Salinity Experiment 2000 and 2001, NW Mediterranean Sea. *Proc. of the First results Workshop: WISE/EuroSTARRS/LOSAC* (pp. 51–59). Toulouse, France: ESA, SP-525.
- François, C., & Ottlé, C. (1994). Estimation of the angular variation of the sea surface emissivity with the ATSR/ERS-1 data. *Remote Sensing of Environment*, 48, 302–308.
- Harris, A. R., Brown, S. J., & Mason, I. M. (1994). The effect of wind speed on sea surface temperature retrieval from space. *Geophysical Research Letters*, 21, 1715–1718.
- Kerr, Y. H., Waldteufel, P., & Berger, M. (2001). Mission Objectives and Scientific Requirements of the Soil Moisture and Ocean Salinity (SMOS) Mission. MRD, ESA: ESTEC, Noordwijk (NL), 44 pp.

- Konda, M., Imasato, N., Nishi, K., & Toda, T. (1994). Measurement of the sea surface emissivity. *Journal of Oceanography*, 50, 17–30.
- Legrand, M., Pietras, C., Brogniez, G., Haeffelin, M., Abuhassan, N. K., & Sicard, M. (2000). A high-accuracy multiwavelength radiometer for in situ measurements in the thermal infrared: Part 1. Characterization of the instrument. *Journal of Atmospheric and Oceanic Technology*, 17, 1203–1214.
- Liu, W. -Y., Field, R. T., Gantt, R. G., & Klemas, V. (1987). Measurement of the surface emissivity of turbid waters. *Remote Sensing of Environment*, 21, 97–109.
- Llewellyn-Jones, D., Edwards, M. C., Mutlow, C. T., Birks, A. R., Barton, I. J., & Tait, H. (2001, February). AATSR: Global-change and surface-temperature measurements from ENVISAT. *ESA Bulletin*, 11–21.
- Masuda, K., Takashima, T., & Takayama, Y. (1988). Emissivity of pure seawaters for the model sea surface in the infrared window regions. *Remote Sensing of Environment*, 24, 313–329.
- Murray, M. J., Allen, M. R., Merchant, C. J., Harris, A. R., & Donlon, C. J. (2000). Direct observations of skin–bulk SST variability. *Geophysical Research Letters*, 27, 1171–1174.
- Niclòs, R., Caselles, V., Coll, C., Valor, E., & Rubio, E. (2004). Autonomous measurements of sea surface temperature using in situ thermal infrared data. *Journal of Atmospheric and Oceanic Technology*, 21(4), 683–692.
- Robinson, I. S., Wells, N. C., & Charnock, H. (1984). The sea surface thermal boundary layer and its relevance to the measurement of surface temperature by airborne and space borne radiometers. *International Journal of Remote Sensing*, 5, 19–46.
- Salisbury, J. W., & D'Aria, D. M. (1992). Emissivity of terrestrial materials in the 8–14 μm atmospheric window. *Remote Sensing of Environment*, 42, 83–106.
- Saunders, P. (1967). The temperature at the ocean–air interface. *Journal of the Atmospheric Sciences*, 24, 267–273.
- Schlüssel, P., Emery, W. J., Grassl, H., & Mammen, T. (1990). On the bulk–skin temperature difference and its impact on satellite remote sensing of sea surface temperature. *Journal of Geophysical Research*, 95(C8), 13341–13356.
- Sicard, M., Spyak, P. R., Brogniez, G., Legrand, M., Abuhassan, N. K., Pietras, C., et al. (1999). Thermal infrared field radiometer for vicarious cross-calibration: Characterization and comparisons with other field instruments. *Optical Engineering*, 38(2), 345–356.
- Sidran, M. (1981). Broadband reflectance and emissivity of specular and rough water surfaces. *Applied Optics*, 20, 3176–3183.
- Smith, W. L., Knuteson, R. O., Revercomb, H. E., Feltz, W., Howell, H. B., Menzel, W. P., et al. (1996). Observations of the infrared radiative properties of the ocean—implications for the measurement of sea surface temperature via satellite remote sensing. *Bulletin of the American Meteorological Society*, 77, 41–51.
- Takashima, T., & Takayama, Y. (1981). Emissivity and reflectance of the model sea surface for the use of AVHRR data of NOAA satellites. *Meteorology and Geophysics*, 32, 267–274.
- Villarino, R., Camps, A., Vall-llossera, M., Miranda, J., Sabia, R., Monerris, A., et al. (2004). Sea surface emission at L-band results from the WISE/FROG field experiments. *Proc. of the International Geoscience and Remote Sensing Symposium. IGARSS '04*. Anchorage, Alaska, in press.
- Watts, P. D., Allen, M. R., & Nightingale, T. J. (1996). Wind speed effects on sea surface emission and reflection for the Along Track Scanning Radiometer. *Journal of Atmospheric and Oceanic Technology*, 13, 126–141.
- Wick, G. A., Emery, W. J., Kantha, L. H., & Schlüssel, P. (1996). The behavior of the bulk–skin sea surface temperature difference under varying wind speed and heat flux. *Journal of Physical Oceanography*, 26, 1969–1988.
- Wu, X., & Smith, W. L. (1997). Emissivity of rough sea surface for 8–13 μm : Modelling and verification. *Applied Optics*, 36, 2609–2619.